Available online at www.sciencedirect.com
SCIENCE DIRECT®
Journal of Magnetic Resonance 162 (2003) 54–66
JMR Journal of Magnetic Resonance
www.elsevier.com/locate/jmr

Band-selective recoupling of homonuclear double-quantum dipolar interaction with a generalized composite 0° pulse: application to ^{13}C aliphatic region-selective magnetization transfer in solids

Yoh Matsuki, Hideo Akutsu, and Toshimichi Fujiwara*

Division of Molecular Biophysics, Institute for Protein Research, Osaka University, 3-2 Yamadaoka, Suita 565-0871, Japan

Received 5 June 2002; revised 6 December 2002

Abstract

Recoupling of homonuclear double quantum (DQ)-dipolar interactions is a useful technique for the structural analysis of molecules in solids. We have designed a series of elemental 0° pulses for the recoupling sequences with the rf phase rotation about the z-axis, known as CN. The proposed 0° pulses whose total flip angle $\geqslant 360°$ provide spin rotation vectors in the xy-plane. Thus, the residual spin rotation can be canceled by rf phase rotation about the z-axis. An analysis by the coherent averaging theory showed that effective bandwidths of the recoupling sequences are limited not by the reduction in the dipolar scaling factor but by the increase in the residual spin rotation due to offset. A CN sequence with these elemental pulses provides an effective bandwidth of DQ-dipolar recoupling from ca. $0.5\nu_R$ to $4\nu_R$ for numerical simulations. Here, ν_R is the sample spinning frequency. The 0° pulses were applied to band-selective recoupling for the magnetization transfer in uniformly ^{13}C-labeled molecules. Narrow-band recoupling enhances the magnetization transfer between spins within the effective range by decoupling the dipolar interactions between spins one of which is outside the range. The narrow band operation reduces rf field strength, which improves the CH decoupling. Increases in signal intensities by the use of the proposed 0° pulses are experimentally shown for ^{13}C-labeled amino acids.

Keywords: Solid-state NMR; Recoupling; Homonuclear double-quantum dipolar interaction; Magic angle sample spinning; Isotope-labeled amino acids

1. Introduction

Solid-state NMR can provide information on structure and dynamics of molecules in non-crystalline states [1,2] and membrane-associated forms [3,4]. Efficient methods for spectral assignment [5–9], inter-nuclear distance measurement [10–14], and dihedral angle determination [15–21] include the use of dipolar interaction restored by rf multi-pulse irradiation under magic angle spinning [22]. Several rf pulse sequences have been designed to recouple zero-quantum (ZQ) [23–28] and double-quantum (DQ) [29–37] components of the homonuclear dipolar interaction. The DQ-dipolar interaction can be recoupled by rotor synchronous rf irradiation that rotates the dipolar spin operators about the B_1 field [9,29,37] or the z-axis in the rotating frame [30–36]. General principles of the rf irradiation symmetry denoted as CN_n^v and RN_n^v allow the latter technique to recouple or decouple the dipolar interaction in homo- and hetero-nuclear spin systems [38–41].

The rf pulse sequence with the CN_n^v symmetry consists of element pulses with rf phase shifts at $2\pi v/N$ steps during n rotor revolutions; here N, v, and n are integers. The symmetries $C7_2^1$ (POST-C7) [32], $C5_2^1$ (SPC5) [33], and $C14_4^5$ (SC14) [35] have been used for the ^{13}C–^{13}C DQ-dipolar recoupling. These sequences are different in required rf amplitude relative to the sample spinning frequency, $\gamma B_1/\omega_R$, but have broad recoupling bandwidths that cover the ^{13}C chemical shifts for organic molecules.

* Corresponding author. Fax: +81-6-6879-8599.
E-mail address: tfjwr@protein.osaka-u.ac.jp (T. Fujiwara).

1090-7807/03/$ - see front matter © 2003 Elsevier Science (USA). All rights reserved.
doi:10.1016/S1090-7807(02)00191-X

The band-selective recoupling can increase the signal sensitivity. It suppresses the interaction with spins outside the effective recoupling range [42]. The narrow band operation can be performed with an rf field amplitude lower than those for broadband operation as shown in [43]. The reduced γB_1 facilitates the CH dipolar decoupling during the recoupling period under a strong rf field for ^{1}H [31].

In this paper, we propose element pulses for efficient band-selective DQ-dipolar recoupling. We have developed element pulses to vary the effective bandwidth of the CN recoupling sequence. A modification of the element pulse in POST-C7 has been shown to improve the tolerance to offset and rf field homogeneity [32]. The pulse we propose is a generalization of that modified pulse. We present an effective Hamiltonian to characterize the offset dependence of the recoupling with the element pulse. Subsequently, the proposed sequences are compared with broadband recoupling sequences. We demonstrate the advantages of the proposed sequences in band-selective magnetization transfer experiments on uniformly ^{13}C-labeled amino acids.

2. Theory

2.1. Off-resonance effects on recoupling of homonuclear DQ-dipolar interaction

In the CN_n^v sequence for recoupling the DQ-dipolar interaction, N cyclic-element pulses are timed to span n rotor revolutions as illustrated in Fig. 1a. Each C-element pulse represents a 0° pulse with a width τ_c. The kth element pulse has a phase $\phi_{rf}^{(k)} = 2\pi vk/N$ $(k = 0, 1, 2\ldots, N-1)$. This rf phase rotation about the z-axis is referred to as the z rotation [32]. It has been verified that the z-rotation symmetries $C7_2^1$, $C5_2^1$, and $C14_4^5$ recouple the homonuclear DQ-dipolar interactions [33,35].

The Hamiltonian in the rotating frame for a dipolar-coupled homonuclear two-spin system under the rf field along the x-axis is expressed as

$$\mathcal{H} = \mathcal{H}_A + \mathcal{H}_B, \tag{1}$$

$$\mathcal{H}_A = \boldsymbol{\omega}_1^{\text{eff}}(t)\cdot\mathbf{I}_1 + \boldsymbol{\omega}_2^{\text{eff}}(t)\cdot\mathbf{I}_2, \tag{2}$$

$$\mathcal{H}_B = \Delta\omega_1^{\text{aniso}}(t)I_{1z} + \Delta\omega_2^{\text{aniso}}(t)I_{2z} + \omega_D(t)(3I_{1z}I_{2z} - \mathbf{I}_1\cdot\mathbf{I}_2), \tag{3}$$

where $\boldsymbol{\omega}_j^{\text{eff}} = (\omega_{rf}(t), 0, \Delta\omega_{jz})$. The isotropic chemical shift and offset are included in $\Delta\omega_{jz}$, and the applied rf field is denoted by $\omega_{rf}(t)$. The time and orientation dependence of the chemical shift anisotropy (CSA) is expressed as

$$\Delta\omega_j^{\text{aniso}}(t) = \sum_{m=-2}^{2}\sum_{n=-2}^{2} A_{2n}^{(j)} D_{n,m}^{(2)}(\Omega_{PR}) d_{m,0}^{(2)}(\theta_{MAS}) \times \exp(im\omega_R t), \tag{4}$$

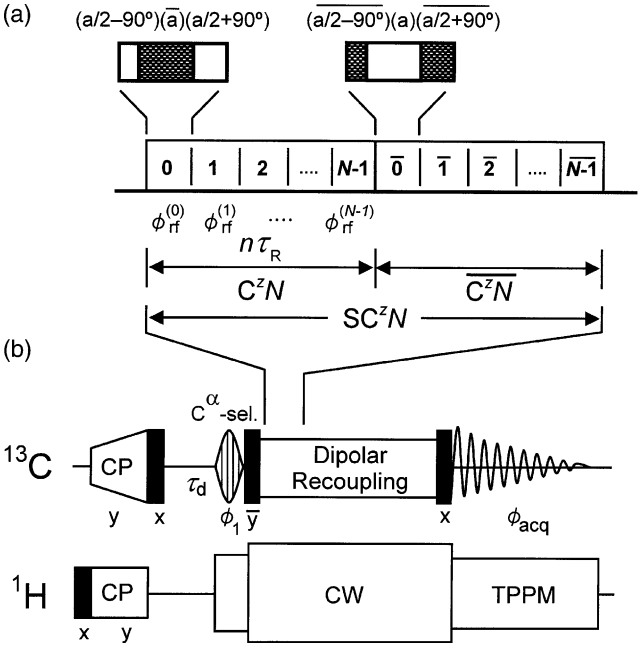

Fig. 1. Pulse sequence SC$^z N$ consisting of the C^z-element pulses for DQ-dipolar recoupling (a), and sequence for selective magnetization transfer (b). (a) The element pulses are phase shifted N times in CN_n^v. The sequence SC$^z N$ denotes C$^z N\overline{C^z N}$. The upper bars represent 180° shifts of the rf phase. In the sequence (b), the ^{13}C magnetization cross-polarized from the ^{1}H magnetization is flipped to the z direction, and the residual transverse components decays during $\tau_d = 10$ ms by the CH dipolar interaction. The dark pulses represent 90° pulses. The Gaussian 90° and the subsequent 90° pulses with a phase cycle prepare the z magnetization only at C$^\alpha$. The z magnetization after the mixing period is read out by the final 90° pulse. The CH dipolar interactions are decoupled by a proton CW field during the recoupling period and by the TPPM sequence during the selective excitation and detection periods. The phase cycles are $\phi_1 = y, \bar{y}$ and $\phi_{acq} = x, \bar{x}$.

where $A_{2n}^{(j)}$ is the spherical tensor element for the chemical shift of spin j, $d_{m,0}^{(2)}(\theta_{MAS})$ is a reduced Wigner rotation matrix element, θ_{MAS} is the magic angle, and $\omega_R = 2\pi/\tau_R$ is the sample-spinning frequency. The Wigner rotation matrices $D_{m,m'}^{(2)}(\Omega_{PR})$ transform the tensor from the principal axis system to the rotor-fixed frame with Euler angles Ω_{PR}. The dipolar coupling strength between the spins is expressed as

$$\omega_D(t) = -\sum_{m=-2}^{2} bD_{0,m}^{(2)}(\Omega_{PR}) d_{m,0}^{(2)}(\theta_{MAS}) \exp(im\omega_R t), \tag{5}$$

with $b = \gamma^2\hbar\mu_0/4\pi r^3$, where γ and r are the gyromagnetic ratio and the internuclear distance, respectively [44].

The propagator for one rf phase modulation cycle $N\tau_c$ is given by

$$U(N\tau_c) = U_A(N\tau_c)U_B(N\tau_c) = \exp(-i\overline{\mathcal{H}}_A N\tau_c)\exp(-i\overline{\mathcal{H}}_B N\tau_c), \tag{6}$$

$$\exp(-i\overline{\mathcal{H}}_A N\tau_c) = \mathcal{T}\exp\left(-i\int_0^{N\tau_c}\mathcal{H}_A(t)\,dt\right), \tag{7}$$

$$\exp(-\mathrm{i}\overline{\mathcal{H}}_{\mathrm{B}}N\tau_{\mathrm{c}}) = \mathcal{T}\exp\left(-\mathrm{i}\int_0^{N\tau_{\mathrm{c}}} U_{\mathrm{A}}^{\dagger}(t)\mathcal{H}_{\mathrm{B}}(t)U_{\mathrm{A}}(t)\,\mathrm{d}t\right), \tag{8}$$

where $\mathcal{T}$ is the Dyson time-ordering operator.

The residual spin rotation due to the offset for the kth C-element pulse in Eq. (7) is expressed as

$$\mathcal{T}\exp\left(-\mathrm{i}\int_{(k-1)\tau_{\mathrm{c}}}^{k\tau_{\mathrm{c}}}\mathcal{H}_{\mathrm{A}}(t)\,\mathrm{d}t\right) = \exp\left(-\mathrm{i}(\omega_1^{\mathrm{eff}}\mathbf{n}_1^{(k)}\cdot\mathbf{I}_1+\omega_2^{\mathrm{eff}}\mathbf{n}_2^{(k)}\cdot\mathbf{I}_2)\tau_{\mathrm{c}}\right), \tag{9}$$

with $\mathbf{n}_j^{(k)}\cdot\mathbf{I}_j = \hat{R}_z(2\pi kn/N)\mathbf{n}_j^{(0)}\cdot\mathbf{I}_j$, where $\hat{R}_z(\phi)\equiv\exp(-\mathrm{i}\phi(\hat{I}_{1z}+\hat{I}_{2z}))$ is a rotation superoperator about the z-axis and $\mathbf{n}_j^{(0)}$ is a rotation axis for the $k=0$ element. When k runs from 0 to $N-1$, the transverse components of the spin operators in Eq. (9) are rotated about the z-axis. Thus the x and y components are averaged out to zero when $\omega_j^{\mathrm{eff}}\tau_{\mathrm{c}}\ll 1$. The resultant effective Hamiltonian is

$$\overline{\mathcal{H}}_{\mathrm{A}} \approx \frac{1}{N\tau_{\mathrm{c}}}\sum_{k=0}^{N-1}\left(\omega_1^{\mathrm{eff}}\mathbf{n}_1^{(k)}\cdot\mathbf{I}_1+\omega_2^{\mathrm{eff}}\mathbf{n}_2^{(k)}\cdot\mathbf{I}_2\right) \approx \omega_1^{\mathrm{eff}}n_{1z}I_{1z}+\omega_2^{\mathrm{eff}}n_{2z}I_{2z}. \tag{10}$$

The lowest order term in the coherent averaging theory would provide a good approximate Hamiltonian for $\overline{\mathcal{H}}_{\mathrm{B}}$ in Eq. (8) as

$$\overline{\mathcal{H}}_{\mathrm{B}} \approx \frac{1}{N\tau_{\mathrm{c}}}\int_0^{N\tau_{\mathrm{c}}} U_{\mathrm{A}}^{\dagger}(t)\mathcal{H}_{\mathrm{B}}(t)U_{\mathrm{A}}(t)\,\mathrm{d}t. \tag{11}$$

Only terms satisfying $mn-\mu v = NZ$ in Eq. (3) are not zero in $\overline{\mathcal{H}}_{\mathrm{B}}$ after averaging over $N\tau_{\mathrm{c}}$, where Z is an integer, m and μ are spatial- and spin-rotation indices in the spherical basis, and v is the number of the phase revolution about the z-axis during the CN sequence. We are interested in the effective Hamiltonian in an offset range where the DQ-dipolar terms are larger than the other terms that are not commutable with the DQ spin operators. Thus we leave only the DQ terms for Eq. (11). The total effective Hamiltonian given by Eq. (6) is

$$\overline{\mathcal{H}}_{\mathrm{eff}}(N\tau_{\mathrm{c}}) \approx \overline{\mathcal{H}}_{\mathrm{A}}+\overline{\mathcal{H}}_{\mathrm{B}}, \tag{12}$$

when higher-order terms are neglected, i.e., $[\overline{\mathcal{H}}_{\mathrm{A}},\overline{\mathcal{H}}_{\mathrm{B}}]N\tau_{\mathrm{c}}\ll\overline{\mathcal{H}}_{\mathrm{A}}+\overline{\mathcal{H}}_{\mathrm{B}}$, and

$$\overline{\mathcal{H}}_{\mathrm{A}} \approx \frac{\omega_\delta}{2}(I_{1z}-I_{2z})+\frac{\omega_\sigma}{2}(I_{1z}+I_{2z}), \tag{13}$$

$$\overline{\mathcal{H}}_{\mathrm{B}} \approx \frac{\omega_{\mathrm{DQ}}}{2}\left(\mathrm{e}^{-\mathrm{i}(\gamma_{\mathrm{PR}}-\chi)}I_1^+I_2^+ + \mathrm{e}^{\mathrm{i}(\gamma_{\mathrm{PR}}-\chi)}I_1^-I_2^-\right), \tag{14}$$

with $\omega_{\mathrm{DQ}}=\kappa b\sin(2\beta_{\mathrm{PR}})$, $\omega_\delta=\omega_1^{\mathrm{eff}}n_{1z}-\omega_2^{\mathrm{eff}}n_{2z}$, and $\omega_\sigma=\omega_1^{\mathrm{eff}}n_{1z}+\omega_2^{\mathrm{eff}}n_{2z}$. Here κ and χ denote the absolute value and the phase of the dipolar scaling factor, respectively. Note that this scaling factor depends on offsets, $\Delta\omega_{1z}$ and $\Delta\omega_{2z}$, as shown in Section C. The supercycle consisting of two CN sequences, C$N\overline{\mathrm{C}N}$ shown in Fig. 1a, further contributes to suppressing the x and y components of $\mathbf{I}_j$ in $\overline{\mathcal{H}}_{\mathrm{A}}$, and does not affect the DQ-dipolar terms recoupled. We neglect terms originating from CSA in Eq. (14), since CSA is suppressed by CN and its supercycles [33].

The effective Hamiltonian in Eq. (12) transfers the magnetization from I_{1z} to I_{2z} as a function of the mixing time τ_m (Appendix A).

$$I_{1z}\xrightarrow{\overline{\mathcal{H}}_{\mathrm{eff}}}(1-\sin^2\phi_{\mathrm{DQ}}\sin^2 q\tau_{\mathrm{m}})I_{1z}-(\sin^2\phi_{\mathrm{DQ}}\sin^2 q\tau_{\mathrm{m}})I_{2z} +\frac{1}{4}\sin 2\phi_{\mathrm{DQ}}(-\cos 2q\tau_{\mathrm{m}}+1)\hat{R}_z\left(\frac{\gamma_{\mathrm{PR}}-\chi}{2}\right)(I_1^+I_2^++I_1^-I_2^-) -\frac{1}{2\mathrm{i}}\sin\phi_{\mathrm{DQ}}\sin 2q\tau_{\mathrm{m}}\hat{R}_z\left(\frac{\gamma_{\mathrm{PR}}-\chi}{2}\right)(I_1^+I_2^+-I_1^-I_2^-), \tag{15}$$

where $\phi_{\mathrm{DQ}}=\arctan(\omega_{\mathrm{DQ}}/\omega_\sigma)$ and $q=\sqrt{\omega_\sigma^2+\omega_{\mathrm{DQ}}^2}/2$. The amplitude of the transferred magnetization is at its maximum at $\tau_{\mathrm{m}}=\pi/2q$. The maximum of the transferred magnetization M_{m} is expressed as a function of $r=\omega_\sigma/\omega_{\mathrm{DQ}}=\omega_\sigma/(\kappa b\sin 2\beta_{\mathrm{PR}})$ by

$$M_{\mathrm{m}}(r)/M_0 = \sin^2\left(\arctan(r^{-1})\right) \approx 1-r^2+\frac{11}{12}r^4-\frac{5}{12}r^6+\cdots, \tag{16}$$

where M_0 is the magnetization for I_{1z} at $\tau_{\mathrm{m}}=0$. Eq. (16) shows that the maximum M_{m} is determined by the pulse sequence through the scaling factor κ and the sum of the z components of the spin rotational frequencies, ω_σ. In an offset range where $r=\omega_\sigma/\omega_{\mathrm{DQ}}<0.5$, M_{m} is larger than about 80% of M_{m} at $\omega_\sigma=0$.

2.2. Composite 0° pulses for band-selective recoupling

Eq. (16) shows that the smaller z component of the residual spin rotation yields larger transferred magnetization. The x and y components of $\omega_j^{\mathrm{eff}}\mathbf{n}_j^{(k)}$ can be canceled by the z rotation as shown in Eq. (10). Thus, the element pulse should have the spin rotation axis $\mathbf{n}_j^{(k)}$ in the xy-plane to maximize the transferred magnetization. To vary the effective bandwidth as a function of the flip angle, we designed a general composite pulses having the rotation axis in the xy-plane.

We start with a phase alternating sequence consisting of two pulses with flip angle a, $(a)_0(a)_\pi$. The net spin rotation angle ϕ_a and its axis $\mathbf{n}_a$ at offset $\Delta\omega_z$ for $(a)_0(a)_\pi$ can be analytically calculated as

$$\mathbf{n}_a = \frac{1}{\sqrt{(1+L)(1-L)}}\begin{pmatrix}0\\-\sin^2(a/2)\sin 2\theta\\-\sin a\cos\theta\end{pmatrix}, \tag{17}$$

$$\phi_a = 2\cos^{-1}L, \tag{18}$$

where $L = \cos^2(a/2) - \sin^2(a/2)\cos 2\theta$ and $\tan\theta = \gamma B_1/\Delta\omega_z$ [45]. Eq. (17) indicates that $(a)_0(a)_\pi$ has the effective rotation axis tilted from the y-axis by ρ in the yz-plane, here

$$\tan\rho = \frac{n_{a,z}}{n_{a,y}} = \frac{\cot(a/2)}{\sin\theta}. \tag{19}$$

This can approximately be solved for ρ under $\Delta\omega_z \ll \gamma B_1$ and $\pi \leqslant a \leqslant 2\pi$ as

$$\rho \approx -\frac{a}{2} - \frac{\pi}{2} + \frac{1}{4}\left(\theta - \frac{\pi}{2}\right)^2 \sin a. \tag{20}$$

The cyclic permutation by $-\rho(>0)$ gave a new C-element pulse, $(\rho + a)_0(a)_\pi(-\rho)_0$. Since $\Delta\omega_z/\gamma B_1 \ll 1$, we can neglect the offset for the permuted pulse. The rotation of the new element pulse is, therefore, expressed as [46]

$$\begin{aligned}
&\exp\left(\mathrm{i}\rho\left(I_x + \frac{\Delta\omega_z}{\gamma B_1} I_z\right)\right)\exp(\mathrm{i}\phi_a \mathbf{n}_a \mathbf{I}) \\
&\quad\times \exp\left(-\mathrm{i}\rho\left(I_x + \frac{\Delta\omega_z}{\gamma B_1} I_z\right)\right) \\
&\quad\approx \exp(\mathrm{i}\rho I_x)\exp(\mathrm{i}\phi_a \mathbf{n}_a \mathbf{I})\exp(-\mathrm{i}\rho I_x) \\
&\quad= \exp\left[\mathrm{i}\phi_a \exp(\mathrm{i}\rho I_x)\mathbf{n}_a \mathbf{I}\exp(-\mathrm{i}\rho I_x)\right].
\end{aligned} \tag{21}$$

Thus the spin rotation axis of this pulse is approximately in the xy-plane. Since $-\rho \approx a/2 + \pi/2$, a generalized C-element pulse that suppresses the z spin rotation component is written as

$$(a/2 - \pi/2)_0(a)_\pi(a/2 + \pi/2)_0. \tag{22}$$

We refer to this element pulse as a C^z-element pulse. The same element pulse at $a = 2\pi$, $(\pi/2)_0(2\pi)_\pi(2\pi/3)_0$, has been used in POST-C7 and SPC5 for the broadband DQ-dipolar recoupling.

We calculate the rotations of a spin by the C^z5 and C^z7 sequences which denote $\mathrm{C}5_2^1$ and $\mathrm{C}7_2^1$ consisting of the C^z-element pulses. Fig. 2 shows the net rotation angle $\phi = 2\omega_j^{\mathrm{eff}}\tau_\mathrm{R}$ and its z component ϕn_z as a function of offset. The offset range where ϕ is suppressed varies with a. The C^z5 sequences reduce the rotational frequency $|\phi n_z/2\tau_\mathrm{R}|$ to less than $0.05\omega_\mathrm{R}$ in the range from -3.0 to $1.0\omega_\mathrm{R}$ at $a = 300°$ and that from -0.4 to $0.4\ \omega_\mathrm{R}$ at $a = 210°$. The z component dominates the spin rotation in the offset range where $\phi \approx \phi n_z$. In this offset range, the approximation to $\overline{\mathcal{H}}_\mathrm{A}$ in Eq. (10) is valid.

The rf field amplitude γB_1 increases with N as $\gamma B_1 = 2Na/n\tau_\mathrm{R}$ when $a/n\tau_\mathrm{R}$ is constant. The net rotation angle of the CN sequence, ϕ, increases with the number of element pulse in the sequence, N, if the spin rotation can be added linearly as shown in Eq. (10). Therefore, the spin rotation of C7 at $\Delta\omega_z/\omega_\mathrm{R}$ is 7/5 times that of C5 at offset (5/7) $\Delta\omega_z/\omega_\mathrm{R}$ as can be seen from Fig. 2. This means that ϕ/N as a function of $\Delta\omega_z/\gamma B_1$ is the same for C5 and C7 as revealed with the upper horizontal and right vertical scales in Fig. 2. Thus, the dependence of ϕ/N on $\Delta\omega_z/\gamma B_1$ for the C^zN sequence is determined not by the symmetry CN but by C^z-element pulse specified by flip angle a.

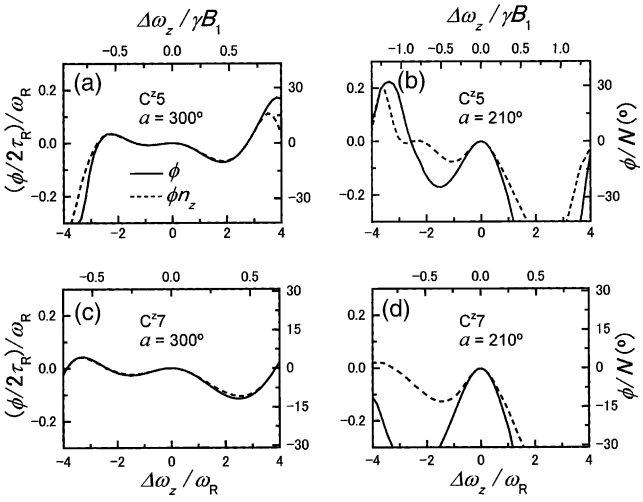

Fig. 2. The residual spin rotational frequency (solid lines) and its z component (broken lines) as a function of offset. The rotations are given for the C^z5 sequence at $a = 300°$ (a) and 210° (b), and the C^z7 sequence at $a = 300°$ (c) and 210° (d). When $\nu_\mathrm{R} = 10\,\mathrm{kHz}$, $\gamma B_1/2\pi$ is 41.7, 29.2, 58.3, and 40.8 kHz for (a), (b), (c), and (d), respectively. The lower horizontal and left vertical axes show scales normalized by ω_R, and the upper horizontal axis shows a scale normalized by γB_1. The vertical axis on the right gives the net spin rotation angle ϕ divided by N.

2.3. Dipolar scaling factor

The absolute value of the scaling factor κ can be factorized as

$$\kappa = \kappa_\mathrm{rf}(a, \mathrm{C}N_n)\kappa_z(\Delta\omega_{1z}, \Delta\omega_{2z}). \tag{23}$$

The factor κ_rf depends on the CN_n symmetry and the element pulse on resonance [39]. The offset also affects κ through κ_z that is normalized to unity at $\Delta\omega_{1z} = \Delta\omega_{2z} = 0$.

The on-resonance scaling factor κ_rf for a C^z-element pulse can be analytically derived as in Appendix B, and its a dependence is shown in Fig. 3. The minimum of κ_rf at $a \approx 270°$, 0.16, is about 30% smaller than the

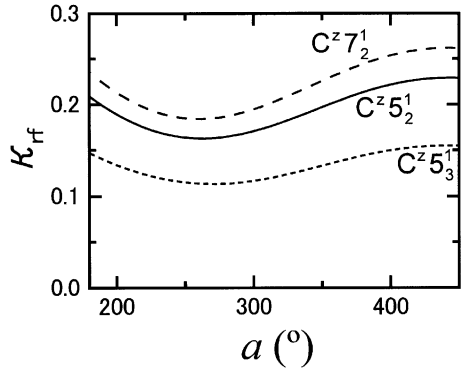

Fig. 3. Scaling factor $\kappa_\mathrm{rf}(a, \mathrm{C}N_n)$ for a C^z-element pulse under the on-resonance condition as a function of flip angle a. Scaling factors for $\mathrm{C}7_2^1$, $\mathrm{C}5_2^1$, and $\mathrm{C}5_3^1$ are shown with broken, solid and dotted lines, respectively.

maximum at $a \approx 450°$, 0.23 for $C^z5^1_2$. The dependence of κ_{rf} on the symmetry is also shown for $C^z5^1_3$ and $C^z7^1_2$.

The offset-dependent factor κ_z was numerically calculated for the SC^z5 sequence at different a. The SC^z5 sequence has the phase modulation used in SPC5 as illustrated in Fig. 1a. Fig. 4 shows κ_z as a function of resonance offsets for the spin pair. The factor κ_z is large along the line $\Delta\omega_{1z} \approx -\Delta\omega_{2z}$ for the element pulse at $a = 300°$ and 340°. The terms proportional to $I_{1z} - I_{2z}$ and $I_{1z} + I_{2z}$ in $\mathcal{H}_A$ are larger along the lines $\Delta\omega_{1z} \approx -\Delta\omega_{2z}$ and $\Delta\omega_{1z} \approx \Delta\omega_{2z}$, respectively. Since $I_{1z} + I_{2z}$ is not commutable with the DQ term but $I_{1z} - I_{2z}$ is, $\mathcal{H}_A$ interferes with the DQ-dipolar recoupling process in Eq. (11) for $\overline{\mathcal{H}}_B$ along the line $\Delta\omega_{1z} \approx \Delta\omega_{2z}$ more than along the line $\Delta\omega_{1z} \approx -\Delta\omega_{2z}$.

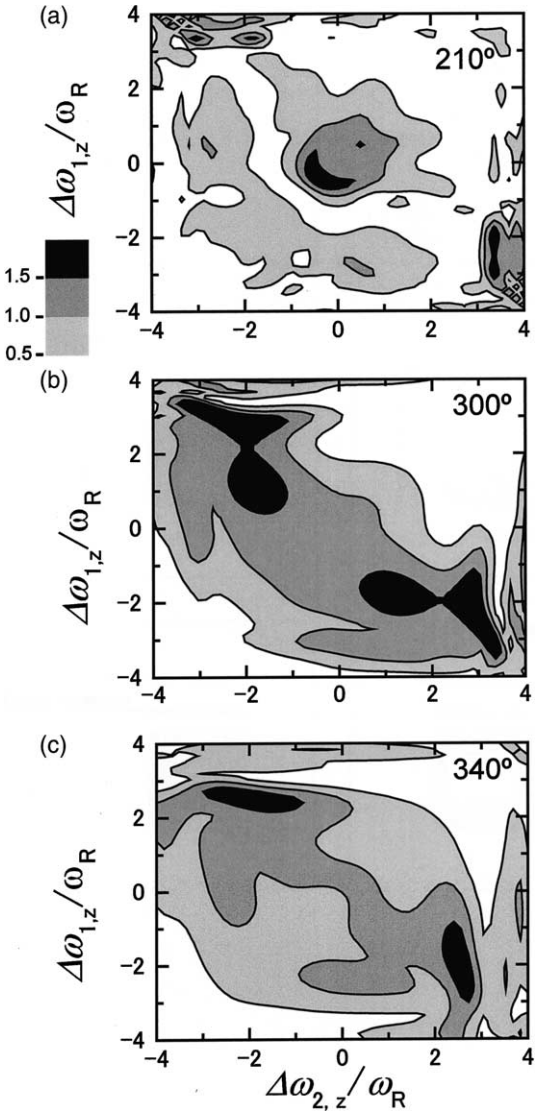

Fig. 4. Contour plots of the scaling factor κ_z as a function of offsets of a pair of carbon spins with an internuclear distance of 0.15 nm. Scaling factors were numerically calculated for the SC^z5 sequence with $a = 210°$ (a), 300° (b), and 340° (c). The regions $\kappa_z \geqslant 0.5$ are shaded as the indicator.

2.4. Off-resonance effects on the magnetization transfer by the DQ-dipolar interaction

The magnetization transfer calculated from the approximate Hamiltonian Eq. (12) qualitatively agrees with that obtained by the exact numerical computation. Fig. 5 shows the offset dependence of the maximum of the magnetization transferred with SC^z5 consisting of the C^z-element pulses at $a = 210°$, 300° and 340° calculated by the two methods. This agreement confirms the validity of the analysis with κ and ω_σ.

The C^z-element pulse maximizes the magnetization transferred by the recoupled dipolar interaction. Fig. 6 shows the maximum transferred magnetization numerically calculated for the SC5 sequence having C-element pulses $(a - x)_0(a)_\pi(x)_0$ for $180° \leqslant a \leqslant 450°$ and $x \leqslant a$ at a constant ω_R. The broken line indicating the C^z condition $x = a/2 + \pi/2$ lies in a shaded region that yields large maxima in the transferred magnetization. The plot for the magnetization has another ridge along $x = (a/2 + \pi/2) - \pi$ which also tilts the rotation axis into the xy-plane.

The offset dependence of $|\omega_\sigma/\kappa_{rf}b|$ for SC^z5 is shown in Fig. 7. Since the magnetization transfer is a function of $\omega_\sigma/\omega_{DQ}$ as shown by Eq. (16), the shaded regions in Figs. 4 ($\kappa_z \geqslant 0.5$) and 7 ($|\omega_\sigma/\kappa_{rf}b| \leqslant 0.5$) exhibit the offset regions favorable for the magnetization transfer. The effective regions in κ_z include those in $|\omega_\sigma/\kappa_{rf}b|$ even for the element pulse at $a = 340°$ which has the largest area $|\omega_\sigma/\kappa_{rf}b| \leqslant 0.5$. This means that the residual spin rotation frequency increases with offset faster than the recoupled DQ-dipolar coupling strength decreases. Therefore, the ratio $\omega_\sigma/\omega_{DQ}$ depends more strongly on ω_σ, and the effective region for the magnetization transfer is limited by ω_σ rather than by κ. This is also confirmed by Fig. 5 showing that the regions where the transferred magnetization is larger than $0.5M_0$ are almost the same as those $|\omega_\sigma/\kappa_{rf}b| \leqslant 0.5$ rather than those $\kappa_z \geqslant 0.5$. Fig. 7 shows $|\omega_\sigma/\kappa_{rf}b|$ for a ^{13}C spin pair at an internuclear distance 0.15 nm. For the pair at a longer distance, the effective offset region is smaller because of larger $|\omega_\sigma/\kappa_{rf}b|$.

As seen in Fig. 7b and c, ω_σ for the element pulses $a = 300°$ and 340° has small absolute value along the anti-diagonal line $\Delta\omega_{1z} \approx -\Delta\omega_{2z}$ as expected from the spin rotation ϕn_z given in Fig. 2. The scaling factor κ_z is large along the $\Delta\omega_{1z} \approx -\Delta\omega_{2z}$ as mentioned for Fig. 4. Thus, the recoupling sequences allow the effective magnetization transfer along the anti-diagonal line.

Because the scaling factor κ is determined by the nutation of the DQ terms due to $\mathcal{H}_A$ within a cycle of a CN sequence as shown by Eq. (11), κ is characterized by the spin dynamics on a time scale shorter than $N\tau_c$. The scaling factor κ depends on the element pulse as well as the symmetry CN^v_n as shown in Fig. 3. Since ω_σ is obtained from the net spin rotations by an entire

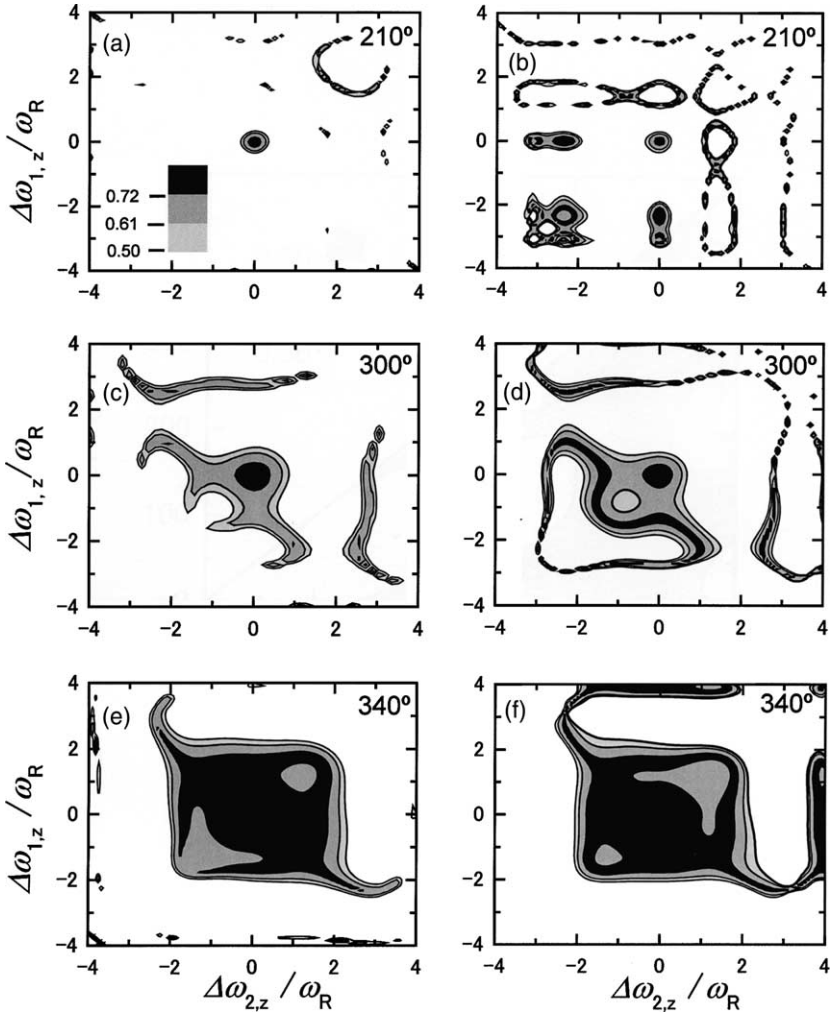

Fig. 5. Contour plots of the maximum transferred magnetization M_m as a function of offsets obtained with the exact numerical computation (a, c, e) and the effective Hamiltonian in Eq. (12) (b, d, f) for the powder distribution. The maximum is shown for the SC^{z}5 sequence with $a = 210°$ (a, b), 300° (c, d), and 340° (e, f). Eq. (16) was used for (b), (d), and (f). Contour lines indicate M_m/M_0.

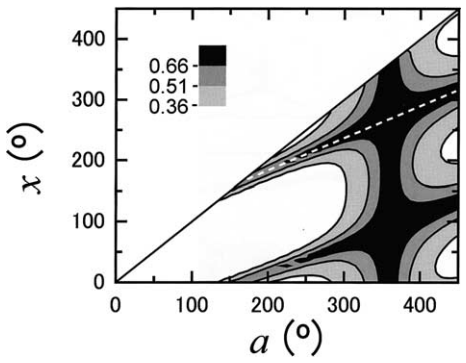

Fig. 6. Maximum transferred magnetization with the SC5 sequence as a function of a and x for the C-element pulse, $(a-x)_0(a)_\pi(x)_0$. The magnetization was numerically calculated for a covalently bonded carbon spin pair at $\nu_R = 10$ kHz in the powdered state. The contour plot gives the maximum transferred magnetization averaged over the offsets $(\Delta\omega_{1z}, \Delta\omega_{2z}) = (0.3, 0.3)\nu_R$, $(0.15, 0.15)\nu_R$, and $(0.15, -0.15)\nu_R$. The white broken line corresponds to the C^z condition, $x = a/2 + \pi/2$. Contour levels indicate the average magnetization normalized by M_0.

recoupling sequence, ω_σ is characterized by the dynamics on a time scale longer than $N\tau_c$ [47]. The element pulse and the supercycle primarily determine ω_σ as mentioned for Fig. 2. For example, the C^z-element pulse at $a = 360°$ used in POST-C7 suppresses ω_σ over an offset range broader than that for $(2\pi)_0(2\pi)_\pi$ in C7 without changing the scaling factor κ_{rf}. The supercycles are also used to cancel ω_σ in SC14 and SPC5.

2.5. Effects of chemical shifts on dipolar spectra

We have examined the effects of the isotropic and anisotropic chemical shifts of the aliphatic carbons on the dipolar scaling and the magnetization transfer. The simulated powder spectra in Fig. 8 show the nutation frequency of the z magnetization by the recoupled dipolar interaction for $^{13}C^{\alpha}$–$^{13}C^{\beta}$ of alanine. The spectrum in Fig. 8a was calculated for the broadband recoupling sequence SPC5, i.e., SC^{z}5 at $a = 360°$. The splitting of

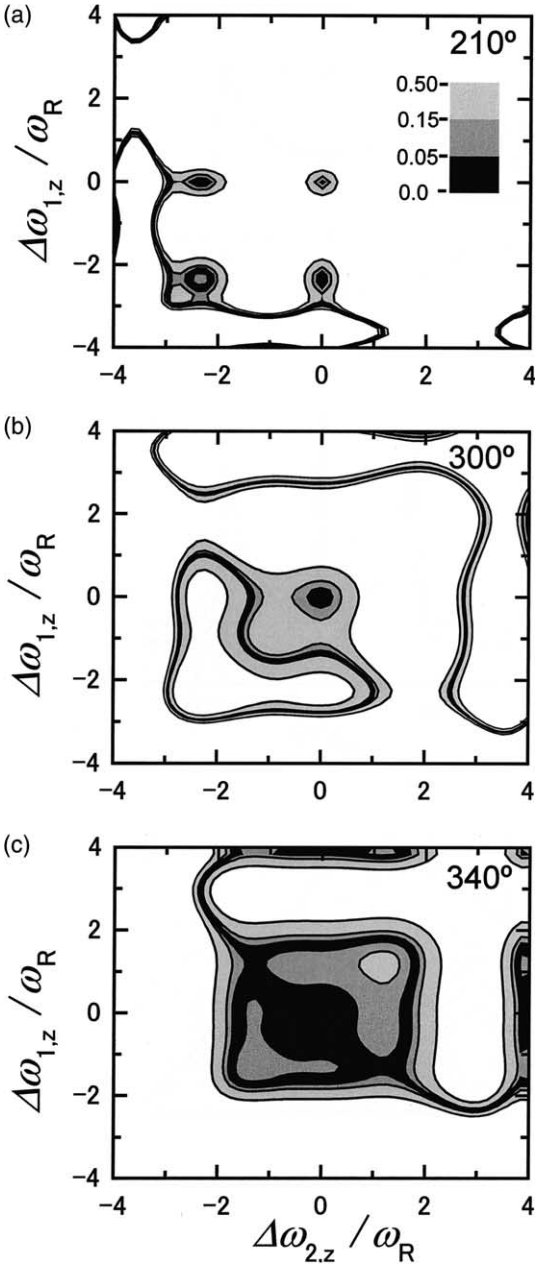

Fig. 7. Contour plots of the spin rotation frequency relative to the dipolar coupling strength $|\omega_\sigma/\kappa_{rf}b|$ as a function of offsets. The relative frequency $|\omega_\sigma/\kappa_{rf}b|$ was calculated for the SC^{z}5 sequence at $a = 210°$ (a), 300° (b), and 340° (c). The offset regions where $|\omega_\sigma/\kappa_{rf}b| \leqslant 0.5$ are shaded as the indicator.

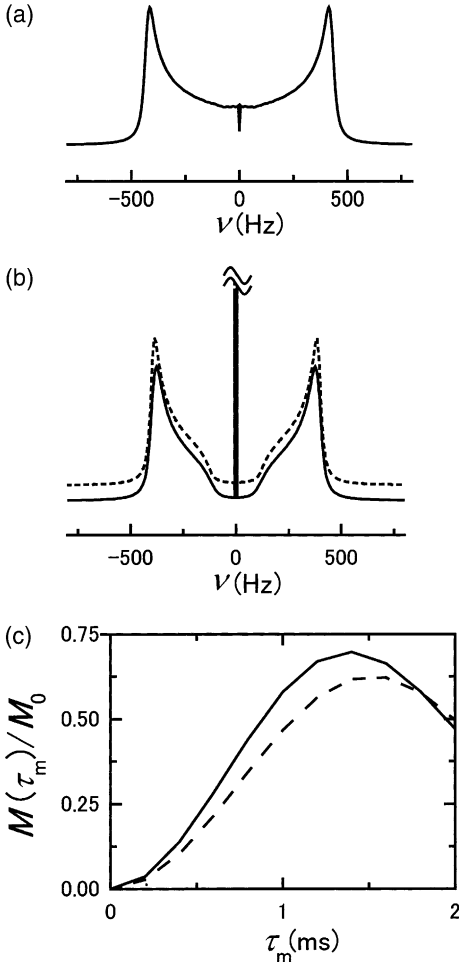

Fig. 8. Dipolar powder spectra for the recoupled DQ-dipolar interaction (a, b), and the transferred magnetization as a function of the mixing time calculated for $^{13}C^{\alpha}$–$^{13}C^{\beta}$ of alanine, (c). The spectra are shown for the SC^{z}5 sequence with $a = 360°$ (a) and 210° (b) at $\nu_R = 10.0$ kHz. The dipolar coupling constant is 2250 Hz. The orientations of the shielding tensors and the principal values for the C^{α} and C^{β} spins were taken from [48]. The spectrum shown with the broken line in (b) was calculated without the shielding anisotropies. The irradiation frequency for the recoupling sequence was set at the center of the two isotropic chemical shifts at $B_0 = 9.4$ T. An exponential line-broadening factor was 32 Hz. Spectra (a) and (b) have the same integral intensity. In (c), the transferred magnetization calculated with parameters used for (a) and (b) is shown with solid and broken lines, respectively. The maxima for the solid and broken lines, are 95% and 85% of the theoretical maximum 0.73, respectively.

the doublet due to the DQ-dipolar coupling is 830 Hz for the spin pair in alanine and 852 Hz for a pair with the identical shift on resonance. The spectrum shown in Fig. 8b was calculated for the narrow-band recoupling sequence SC^{z}5 at $a = 210°$. The splitting of the spectrum is 752 Hz for alanine and 820 Hz for the spin pair with the identical shift on resonance. The spectrum shown by the broken line in Fig. 8b was calculated for SC^{z}5 at $a = 210°$ without the chemical shift anisotropy. The small difference between the spectra indicates effects of the anisotropy are negligible. Thus the isotropic chemical shifts for alanine reduce the effective coupling by less than 10%.

The isotropic chemical shifts suppress the spectral intensity near zero frequency and give the strong peak at zero frequency as shown in Fig. 8b. The frequency of the z field, ω_σ, is about 130 Hz, which can be obtained from the sum of the z-rotation frequencies at offset about 1.5 and −1.5 kHz in Fig. 2b. Eq. (15) indicates that such ω_σ yields a nutation component with frequency $2q$ and amplitude proportional to $\sin^2\phi_{DQ}$. Since $2q \geqslant \omega_\sigma$, the spectral intensity less than $\nu \approx 130$ Hz is eliminated.

Fig. 8c shows the influence of the chemical shifts on the magnetization transfer. The effective bandwidth of the SC^{z}5 sequence at $a = 210°$ is about one-sixth of that at $a = 360°$. This reduction in the bandwidth is accompanied by a decrease in the maximum transferred magnetization only by about 10%. The decreased transfer is due to the z field mainly caused by the isotropic chemical shifts.

3. Experimental

3.1. NMR experiments

Experiments were performed on a Varian Infinity-400 spectrometer at a ^{13}C resonance frequency of 100.1 MHz with a broadband double-resonance MAS probe for a 4-mm spinner. Only the spectra in Fig. 10 were obtained with an Infinity plus-500 spectrometer at a ^{13}C frequency of 125.7 MHz. The carbon magnetization was prepared by cross-polarization with the ^{13}C ramped rf amplitude from 55 to 65 kHz at $\nu_R = 10$ kHz and from 50 to 60 kHz at $\nu_R = 15$ kHz under the ^{1}H field amplitude of 70 kHz [51]. The amplitudes of 90° pulses were 70 kHz for ^{1}H and ^{13}C. The Gaussian selective pulse consisted of 17 rectangular pulses of 4 μs width separated by 40 μs intervals. The pulse sequences for Fig. 10b–d had a delay of $1/\nu_R$ without the CH decoupling field immediately after the recoupling sequence. The spinning frequency was kept within a deviation of 0.1%. Proton CW decoupling during the recoupling period was 100 kHz in $\gamma B_1/2\pi$. The TPPM decoupling [52] during the selective excitation and detection periods consisted of 170° pulses at a field strength of 85 kHz with a phase excursion of ±7°. The samples were uniformly 95% ^{13}C, ^{15}N-labeled L-alanine and L-valine (Shoko, Japan) diluted to 10% and 50%, respectively, with natural abundance alanine and valine. The amounts of carbon-13 nuclei in the natural abundance and enriched samples were taken into account to evaluate the transferred magnetization.

3.2. Numerical simulation

The time evolution of the spin system was calculated by the numerical integration of a time-dependent Hamiltonian including terms for the ^{13}C-dipolar interactions, the isotropic and anisotropic chemical shifts, and the rf field. A total propagator for a 2π sample rotation was expressed as a product of about 100 element propagators that were calculated on the assumption of the time independence during the short piecewise sections. The time-domain signals for about 1300 orientations were summed up to reproduce the powder distribution. The transferred magnetization as a function of the mixing time was computed as

$$M(\tau_m) = \frac{M_0}{8\pi^2}\int_0^{2\pi}\int_0^{\pi}\int_0^{2\pi} \mathrm{Tr}\{I_{2z}U(\tau_m)I_{1z}U^{\dagger}(\tau_m)\} \times d\alpha_{PR}\sin\beta_{PR}\,d\beta_{PR}\,d\gamma_{PR}. \quad (24)$$

The dipolar spectra in Fig. 8 were obtained by the Fourier transformation of the time-dependent sum magnetization, $I_{1z} + I_{2z}$, under the recoupling sequence for about 35×10^5 orientations. All numerical simulation programs coded in FORTRAN were run on an SGI Origin200 workstation having four R10000 processors.

4. Experimental results

Advantages in using the band-selective recoupling sequences with the C^z-element pulses are demonstrated. The spectra shown in Fig. 9 were obtained with the sequence in Fig. 1b for monitoring the z magnetization transfer by the recoupled DQ-dipolar interactions. Fig. 9b shows that the dipolar couplings transfer the $^{13}C^{\alpha}$ magnetization to $^{13}C^{\beta}$ and ^{13}CO under the broadband sequence SPC5 in uniformly labeled L-alanine at $\nu_R = 10$ kHz. The irradiation frequency of SPC5 and the mixing time were selected so that they maximized the magnetization transferred to C$^{\beta}$ for Fig. 9c. We made band-selective recoupling experiments to optimize the transfer to C$^{\beta}$ by using the SC^{z}5 sequence at $a = 210°$. The maximum of the magnetization transferred to C$^{\beta}$ with the band-selective sequence (Fig. 9d) was 25% larger than that with the broadband sequence (Fig. 9c). This enhancement under the selective sequence is due to decoupling of the ^{13}C–^{1}H dipolar interactions as well as unnecessary ^{13}C–^{13}C interactions. The selective operation decouples dipolar interaction between ^{13}C spins one of which is outside the effective range and permits the magnetization transfer only within the effective range. The SC^{z}5 sequence at $a = 210°$ needs a ^{13}C rf field amplitude of 29.2 kHz which is smaller than the amplitude for SPC5, 50.0 kHz. This smaller recoupling field amplitude aids decoupling the CH dipolar interactions.

The C^z-element pulse can be used at faster sample spinning rates to increase the transferred magnetization in the aliphatic spectral region. We compared the SC^{z}5 sequence at $a = 210°$ with SC14 whose mixing field amplitude is 1.4 times smaller than that of SPC5. As shown in Fig. 10b, the DQ-dipolar interaction recoupled under SC14 transferred the magnetization from C$^{\alpha}$ to all the other ^{13}C spins in uniformly labeled L-valine at $\nu_R = 15$ kHz. The irradiation frequency and the mixing time were adjusted in order to maximize the magnetization transferred to C$^{\beta}$. Fig. 10c shows that the narrow bandwidth for SC^{z}5 at $a = 210°$ increased the magnetization transferred from C$^{\alpha}$ to C$^{\beta}$ and C$^{\gamma}$ by excluding the carboxyl ^{13}C from the ^{13}C dipolar coupled spin network. It is also possible to find a pulse width and an rf field frequency experimentally that allow the

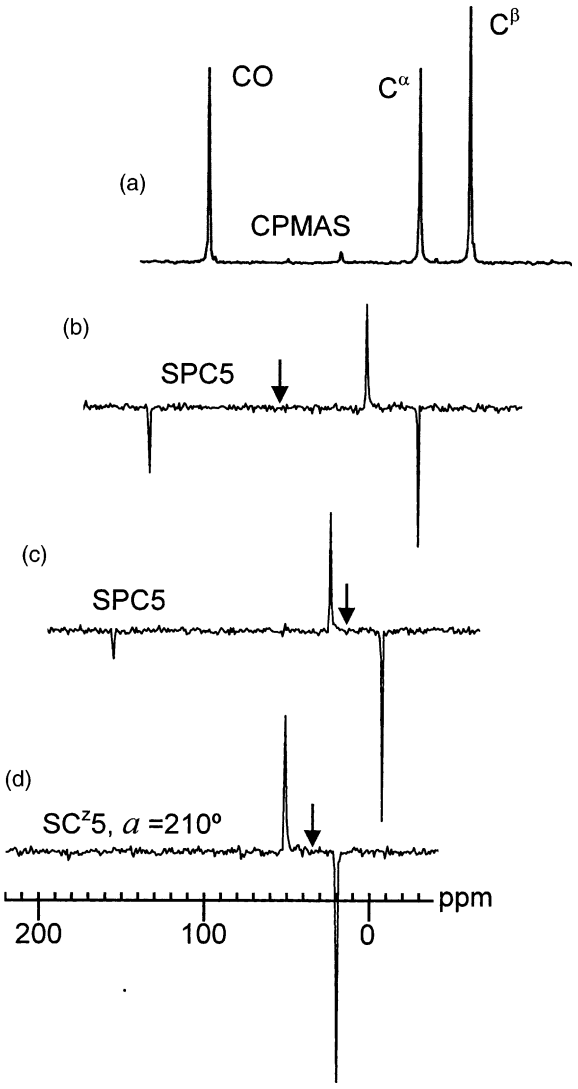

Fig. 9. Spectra of uniformly ^{13}C, ^{15}N-labeled L-alanine obtained with cross-polarization (a) and the pulse sequence shown in Fig. 1b (b–d) at $\nu_R = 10\,kHz$ and $B_0 = 9.4\,T$. The SC^z5 recoupling sequences having $a = 360°$ (b, c) and 210° (d) were employed with $\gamma B_1/2\pi = 50.0$ and 29.2 kHz, respectively, and a mixing time of 1.2 ms. The spectra in (b–d) are shown with the same gain for signal intensity. Arrows indicate the irradiation frequency.

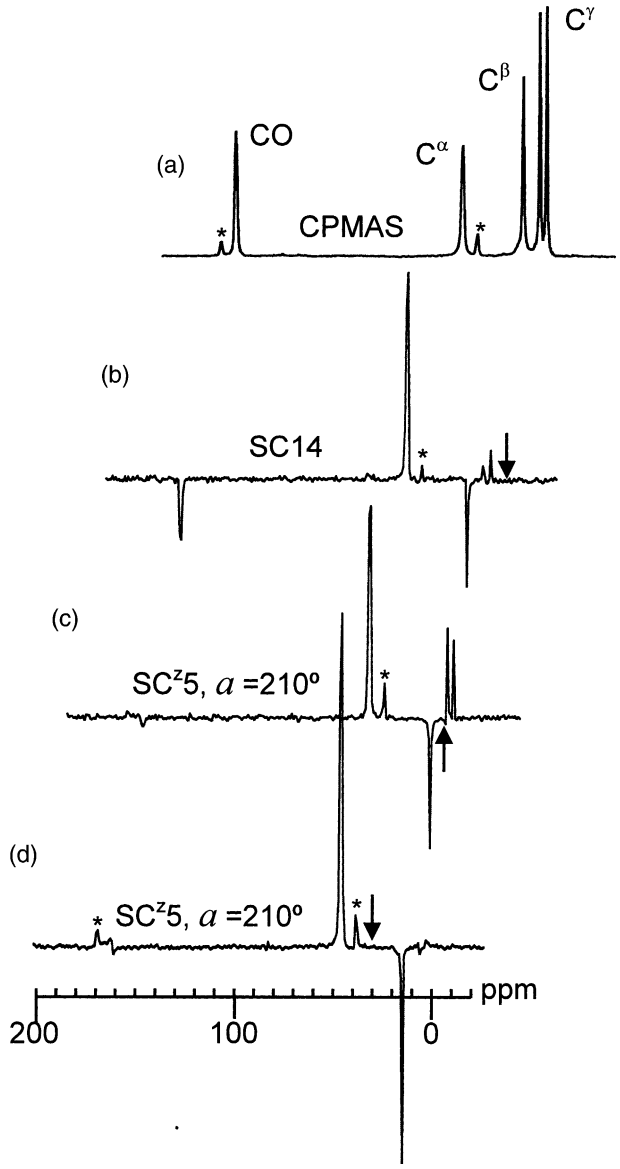

Fig. 10. Spectra of uniformly ^{13}C, ^{15}N-labeled L-valine obtained with cross-polarization (a) and the pulse sequence shown in Fig. 1b (b–d) at $\nu_R = 15\,kHz$ and $B_0 = 11.8\,T$. The SC14 sequence (b) and the SC^z5 sequence with $a = 210°$ (c, d) were used in the recoupling period. The mixing time was 0.80, 1.60, and 1.06 ms for (b), (c), and (d), respectively. The recoupling field amplitude was 52.5 kHz (b) and 43.8 kHz (c, d). The spectra (b–d) are shown with the same gain for signal intensity. Asterisks indicate spinning sidebands.

magnetization transfer only between C^α and C^β as shown in Fig. 10d. The magnetization transferred from C^α to C^β with the SC^z5 sequence was maximized. The magnetization transferred to C^β with SC^z5 at $a = 210°$ is twice as large as that with SC14 (Fig. 10b). This enhancement would partly be due to the improved CH dipolar decoupling, because the rf field amplitude of the SC^z5 sequence, 43.8 kHz, is smaller than that of SC14, 52.5 kHz.

Fig. 11 shows the offset dependence of the magnetization transferred from C^α to C^β in alanine at $\nu_R = 10\,kHz$ obtained with experiments and numerical simulations for the ^{13}C three-spin system. The SC^z5 sequence at $a = 210°$ has the bandwidth of about $0.5\omega_R$ at $\gamma B_1 = 2.9\omega_R$ as shown in Fig. 11a. In Fig. 11c, the SC^z5 sequence at $a = 340°$ has the broadest bandwidth of about 3.0 ω_R at $\gamma B_1 = 4.7\omega_R$. This bandwidth is slightly larger than that for SPC5 (Fig. 11d) at $\nu_R = 10\,kHz$. The experimental magnetization was lower than calculated one at $a \geqslant 300°$, probably because of experimental imperfections such as residual CH dipolar interactions and rf inhomogeneity. We have also calculated the effect of ±5% rf field inhomogeneity on the transfer efficiency. The homogeneity does not have significant effects as shown by Fig. 11.

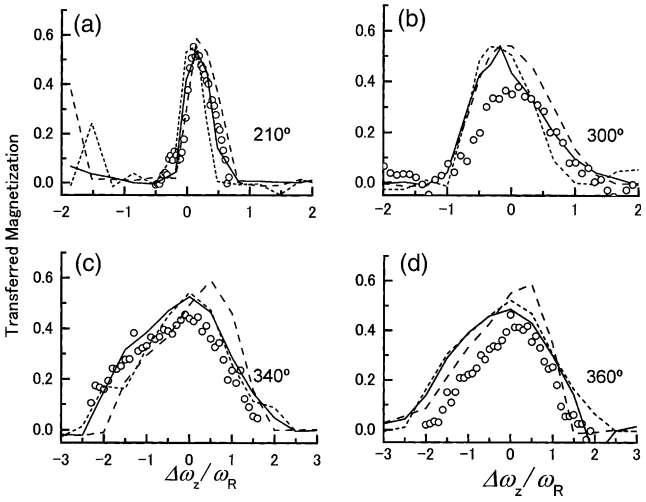

Fig. 11. The experimental (circles) and calculated (lines) magnetization transferred with SC^z5 at $a = 210°$ (a), 300° (b), 340° (c), and 360° (d) as a function of offset for fully ^{13}C-labeled alanine at $\nu_R = 10$ kHz. The rf amplitude was 29.2 (a), 41.7 (b), 47.2 (c), and 50.0 kHz (d). The numerical simulations were performed for the three-spin system $^{13}C^{\alpha}\_^{13}C^{\beta}\_^{13}CO$ in alanine. The calculated intensities of the magnetization at +5% and −5% rf inhomogeneity are also shown in each figure by broken and dotted lines, respectively. The transferred magnetization was measured from the integral intensity of the C^{β} signal. The mixing time was 1.2 ms.

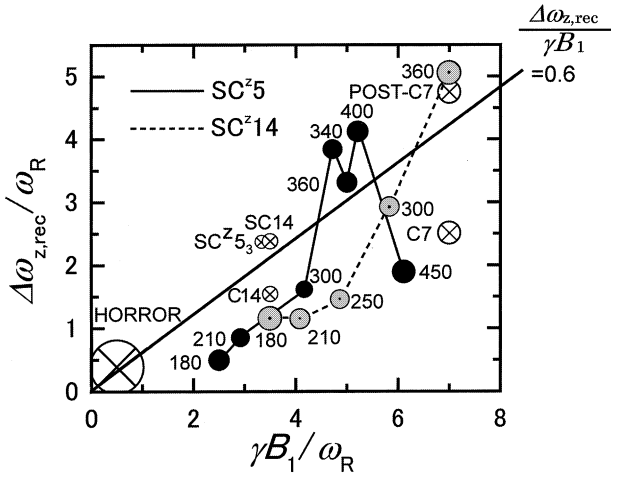

Fig. 12. Effective bandwidth, $\Delta\omega_{z,rec}/\omega_R$, as a function of the recoupling field amplitude, $\gamma B_1/\omega_R$, calculated for DQ-dipolar recoupling sequences. The solid and broken lines connect the points obtained for SC^z5 and SC^z14, respectively. The C-element pulse in SC14 and $C14^5_4$ is $(2\pi)_0$ and that in $SC^z5_3 = C5^1_3\overline{C5^1_3}$ is $(\pi/2)_0(2\pi)_\pi(3\pi/2)_0$. The effective bandwidths were computed for a covalently bonded ^{13}C pair with the same resonance frequency. The effective recoupling bandwidth $\Delta\omega_{z,rec}$ is defined by the offset range where the maximum transferred magnetization M_m is larger than a half of M_m on resonance. Effective bandwidths were calculated at $\nu_R = 10$ kHz, but they were almost the same at 20 kHz in the scale normalized by ω_R. The radii of the circles are proportional to the scaling factors.

5. Discussion

Faster sample spinning rates are necessary for reducing spinning sidebands at higher static magnetic fields and suppress ^{13}C–^{13}C dipolar couplings during the detection period. The faster spinning rates increase γB_1 that is applied synchronously with the sample spinning. However, a lower rf field amplitude is preferable for the CH decoupling and the reduction of the load on probe circuits. The recoupling field amplitude required for the CN sequence is determined as $\gamma B_1 = \omega_R(\theta_{tot}/2\pi)N/n$. This equation shows that γB_1 can be reduced by decreasing the ratio N/n of the CN symmetry and/or the total flip angle θ_{tot} of the element pulse. The symmetries $C5^1_2$ employed in SPC5 and $C5^1_3$ reduce γB_1 for C7 by factors of 1.4 and 2.1, respectively. The C-element pulse $(2\pi)_0$ used in SC14 is twice shorter in θ_{tot} than that used in POST-C7, $(\pi/2)_0(2\pi)_\pi(3\pi/2)_0$, thereby reduces γB_1. The C^z-element pulses also reduce γB_1 with smaller θ_{tot}, when the required recoupling bandwidth is smaller than the effective recoupling bandwidth of SC^z5 and C^z7 at $a = 360°$. The proposed C^z-element pulses can be combined with any CN symmetries.

We compare recoupling sequences in Fig. 12 which exhibits effective bandwidths for DQ-dipolar recoupling as a function of $\gamma B_1/\omega_R$. The radii of the circles give the scaling factors for reference. The efficiency of the recoupling sequence can be measured by the effective bandwidth relative to γB_1 under complete CH dipolar decoupling. Recoupling sequences with the effective bandwidths $\Delta\omega_{z,rec}/\gamma B_1 > 0.6$ are relatively efficient. The sequences SC^z14 at $a = 360°$, POST-C7, SC^z5 at $a = 340$–$400°$, SC^z5_3, SC14, and HORROR are located in the efficient region. The pulse sequences SC^z14 at $a = 360°$ and POST-C7 need a high $\gamma B_1/\omega_R$ and have the broadest effective bandwidth, $5.0\omega_R$. The sequences SC^z5 at $a = 340°$ and SC14 have effective bandwidths of 4.0 and $2.5\omega_R$, respectively, at lower $\gamma B_1/\omega_R$. The C^z element specified by a makes the SC^z14 and SC^z5 sequence band-selective in a range from 5.0 to $0.5\omega_R$ as shown by the lines in Fig. 12. The efficiency of the C^zN sequence becomes small as the effective bandwidth decreases. Finally, HORROR is an efficient selective method with a bandwidth $0.5\omega_R$ [29]. Numerical simulation at 0, ±5 and ±10% rf field inhomogeneity indicated HORROR was more sensitive to the homogeneity than C^zN at $a = 210°$ in magnetization transfer (data not shown). HORROR has practically been used with the adiabatic sweep of the field strength to compensate for the resonance offset and rf field inhomogeneity [37]. Thus this adiabatic recoupling method needs a longer mixing time though HORROR has the highest scaling factor.

6. Conclusions

We have shown that the sum of the z-rotation frequencies ω_σ and the scaling factor κ characterize

the DQ-dipolar recoupling with the CN sequence. The theory and simulations revealed that the offset dependence of the DQ-dipolar recoupling is primarily determined by ω_σ. For example, the recoupling pulse sequence SC^{z}5 consisting of the proposed C^z-element pulses can vary the bandwidth of the offset range where ω_σ is suppressed, yielding the effective recoupling bandwidth between $0.5\omega_R$ and $4\omega_R$ as a function of flip angle a.

These band-selective sequences can be applied to the correlation experiments on ^{13}C-labeled aliphatic carbons in peptides and proteins for the signal assignment. The band-selective recoupling sequences are capable of limiting the propagation of the magnetization in the dipolar-coupled spin network and necessitate smaller γB_1. Consequently, the magnetization transferred with the selective sequence SC^{z}5 was larger than that with the broadband sequences SPC5 and SC14 as shown by the experimental spectra in Figs. 9 and 10. The selective mixing would also be advantageous in obtaining higher resolution along the indirect detection axes in multi-dimensional spectra, because it can suppress aliasing of signals outside the effective region. The selective recoupling of the DQ-dipolar interaction is useful for spins with chemical shift differences much smaller than ω_R. This selective recoupling is, therefore, complementary to RFDR [25,26,28] and narrowband RFDR [27] which favor the magnetization transfer for spin pairs with resonance frequency differences comparable to ω_R. The proposed sequences can also be applied to the INADEQUATE [33,49] and DQ filter experiments [50].

Acknowledgments

This research was partially supported by Grant-in-Aids for Scientific Research from the Ministry of Education and Science and by grants from the Japan New Energy and Industrial Technology Development Organization and Yokohama City Collaboration of Regional Entities for the Advancement of Technological Excellence, JST (H.A.).

Appendix A. Magnetization transfer under the effective Hamiltonian

The magnetization transfer under the effective Hamiltonian of Eq. (12) is analytically derived. The effective Hamiltonian is expressed as

$$\overline{\mathcal{H}}_{\text{eff}} = \omega_\delta I_z^{(23)} + \omega_\sigma I_z^{(14)} + \omega_{\text{DQ}} \hat{R}_z^{(14)}(\gamma_{\text{PR}} - \chi) I_x^{(14)}, \quad \text{(A.1)}$$

with the superoperator $\hat{R}_z^{(14)}(\varepsilon) \equiv \exp(-\mathrm{i}\varepsilon \hat{I}_z^{(14)})$ and single transition operators,

$$I_z^{(23)} = \frac{1}{2}(I_{1z} - I_{2z}), \quad I_z^{(14)} = \frac{1}{2}(I_{1z} + I_{2z}),$$
$$I_x^{(14)} = \frac{1}{2}(I_1^+ I_2^+ + I_1^- I_2^-), \quad I_y^{(14)} = \frac{1}{2\mathrm{i}}(I_1^+ I_2^+ - I_1^- I_2^-). \quad \text{(A.2)}$$

This Hamiltonian can be diagonalized by the unitary transformation

$$U = \exp(-\mathrm{i}\phi_{\text{DQ}} I_y^{(14)}), \quad \text{(A.3)}$$

with $\phi_{\text{DQ}} = \arctan(\omega_{\text{DQ}}/\omega_\sigma)$, and has four eigenvalues,

$$E_1 = \frac{1}{2}\sqrt{\omega_\sigma^2 + \omega_{\text{DQ}}^2} = q, \quad E_2 = \frac{1}{2}\omega_\delta,$$
$$E_3 = -\frac{1}{2}\omega_\delta, \quad E_4 = -q. \quad \text{(A.4)}$$

Here, the energy difference $E_1 - E_4 = 2q$ determines the evolution frequency under the recoupled DQ-dipolar interaction.

The time-dependence of the magnetization during the mixing period can be expressed as a rotation of the density operator in DQ subspace at the frequency $2q$ about an axis inclined from $I_z^{(14)}$ by ϕ_{DQ} in the plane formed by $I_x^{(14)}$ and $I_z^{(14)}$ at $\gamma_{\text{PR}} - \chi = 0$. When the initial state is I_{1z}, the propagator for $\mathcal{H}_{\text{eff}}$, U_{eff}, provides the density operator at the mixing time τ_m as

$$\sigma(\tau_m) = U_{\text{eff}}(\tau_m) I_{1z} U_{\text{eff}}(\tau_m)^{-1}. \quad \text{(A.5)}$$

The time dependence of the magnetization transferred from I_{1z} to I_{2z} is written as

$$\text{Tr}\{I_{2z}\sigma(\tau_m)\} = -\sin^2\phi_{\text{DQ}} \sin^2 q\tau_m. \quad \text{(A.6)}$$

Thus the transferred magnetization reaches the maximum in amplitude, $\sin^2\phi_{\text{DQ}}$, at $\tau_m = \pi/2q$. Similar relations are found for the magnetization transfer in the ZQ subspace [53].

Appendix B. Scaling factors

We derive the scaling factor on resonance for the CN sequence consisting of C-element pulses expressed by $(a-x)_0(a)_\pi(x)_0$. The scaling factor for the DQ-dipolar term with $\mu = 2$ and m is defined as

$$\kappa_{\text{rf}} \mathrm{e}^{\mathrm{i}\chi} = \frac{1}{\tau_c}\int_0^{\tau_c} d_{20}^{(2)}(\beta_{\text{rf}}(t)) \mathrm{e}^{\mathrm{i}m\omega_R t}\,\mathrm{d}t, \quad \text{(B.1)}$$

where κ_{rf} and χ represent the absolute value and the phase of the scaling factor [39]. When the time-dependent spin rotation angle $\beta_{\text{rf}}(t)$ is written as

$$\beta_{\text{rf}}(t) = \begin{cases} 2a\frac{t}{\tau_c} & \text{if } 0 \leqslant t < f\tau_c, \\ 2a(2f - \frac{t}{\tau_c}) & \text{if } f\tau_c \leqslant t < (f+0.5)\tau_c, \\ 2a(\frac{t}{\tau_c} - 1) & \text{if } (f+0.5)\tau_c \leqslant t < \tau_c, \end{cases} \quad \text{(B.2)}$$

with $f = (a - x)/2a$, the scaling factor κ_{rf} is given by

$$\kappa_{\mathrm{rf}} = \frac{3}{4\sqrt{2}} \times \frac{aN^2}{(2aN)^2 - (mn\pi)^2} \times \sqrt{A^2 + B^2}, \tag{B.3}$$

where

$$A = \frac{aN}{n\pi} \sin\left(\frac{2\pi mn}{N}\right) - \sin(4af)\cos\left(f\frac{2\pi mn}{N}\right) + \sin(4af - 2a)\cos\left((f + 0.5)\frac{2\pi mn}{N}\right), \tag{B.4}$$

$$B = \frac{aN}{n\pi}\left(1 - \cos\left(\frac{2\pi mn}{N}\right)\right) - \sin(4af)\sin\left(f\frac{2\pi mn}{N}\right) + \sin(4af - 2a)\sin\left((f + 0.5)\frac{2\pi mn}{N}\right). \tag{B.5}$$

These equations for A and B are reduced to

$$\kappa_{\mathrm{rf}} = \frac{3}{8\sqrt{2}} \times \frac{N^3}{\pi(4N^2 - 1)} \times \sqrt{\sin^2\left(\frac{4\pi}{N}\right) + \left\{1 - \cos\left(\frac{4\pi}{N}\right)\right\}^2} \tag{B.6}$$

at $(a, x) = (360°, 270°), m = 1$, and $n = 2$. This result, Eq. (B.6), agrees with the scaling factor obtained previously [32].

References

[1] F.J. Blanco, S. Hess, L.K. Pannell, N.W. Rizzo, R. Tycko, Solid-state NMR data support a helix–loop–helix structural model for the N-terminal half of HIV-1 Rev in fibrillar form, J. Mol. Biol. 313 (2001) 845–859.

[2] T.S. Burkoth, T.L.S. Benzinger, V. Urban, D.M. Morgan, D.M. Gregory, P. Thiyagarajan, R.E. Botto, S.C. Meredith, D.G. Lynn, Structure of the β-amyloid$_{(10-35)}$ fibril, J. Am. Chem. Soc. 122 (2000) 7883–7889.

[3] H.J.M. de Groot, Solid-state NMR spectroscopy applied to membrane proteins, Curr. Opin. Struct. Biol. 10 (2000) 593–600.

[4] J. Kikuchi, M.P. Williamson, K. Shimada, T. Asakura, Structure and dynamics of photosynthetic membrane-bound proteins in *Rhodobacter Sphaeroides*, studied with solid-state NMR spectroscopy, Photosynth. Res. 63 (2000) 259–267.

[5] T. Fujiwara, K. Sugase, M. Kainosho, A. Ono, A.(M.) Ono, H. Akutsu, ^{13}C–^{13}C and ^{13}C–^{15}N dipolar correlation NMR of uniformly labeled organic solids for the complete assignment of their ^{13}C and ^{15}N signals: an application to adenosine, J. Am. Chem. Soc. 117 (1995) 11351–11352.

[6] C.M. Rienstra, M. Hohwy, M. Hong, R.G. Griffin, 2D and 3D ^{15}N–^{13}C–^{13}C NMR chemical shift correlation spectroscopy of solids: assignment of MAS spectra of peptides, J. Am. Chem. Soc. 122 (2000) 10979–10990.

[7] A. McDermott, T. Polenova, A. Bockmann, K.W. Zilm, E.K. Paulsen, R.W. Martin, G.T. Montelione, Partial NMR assignments for uniformly (^{13}C, ^{15}N)-enriched BPTI in the solid state, J. Biomol. NMR 16 (2000) 209–219.

[8] B.-J. van Rossum, F. Castellani, K. Rehbein, J. Pauli, H. Oschkinat, Assignment of the nonexchanging protons of the α-spectrin SH3 domain by two- and three-dimensional ^{1}H–^{13}C solid-state magic-angle spinning NMR and comparison of solution and solid-state proton chemical shifts, Chembiochem. 2 (2001) 906–914.

[9] A. Detken, E.H. Hardy, M. Ernst, M. Kainosho, T. Kawakami, S. Aimoto, B.H. Meier, Methods for sequential resonance assignment in solid, uniformly ^{13}C, ^{15}N labeled peptides: quantification and application to antamanide, J. Biomol. NMR 20 (2001) 203–221.

[10] O.B. Peersen, M. Groesbeek, S. Aimoto, S.O. Smith, Analysis of rotational resonance magnetization exchange curves from crystalline peptides, J. Am. Chem. Soc. 117 (1995) 7228–7237.

[11] D.R. Studelska, C.A. Klug, D.D. Beusen, L.M. McDowell, J. Schaefer, Long-range distance measurements of protein binding sites by rotational-echo double-resonance NMR, J. Am. Chem. Soc. 118 (1996) 5476–5477.

[12] S. Kiihne, M.A. Mehta, J.A. Stringer, D.M. Gregory, J.C. Shiels, G.P. Drobny, Distance measurements by dipolar recoupling two-dimensional solid-state NMR, J. Phys. Chem. A 102 (1998) 2274–2282.

[13] C.A. Fyfe, A.R. Lewis, Investigation of the viability of solid-state NMR distance determinations in multiple spin systems of unknown structure, J. Phys. Chem. B 104 (2000) 48–55.

[14] O.J. Murphy III, F.A. Kovacs, E.L. Sicard, L.K. Thompson, Site-directed solid-state NMR measurement of a ligand-induced conformational change in the serine bacterial chemoreceptor, Biochemistry 40 (2001) 1358–1366.

[15] Y. Ishii, T. Terao, M. Kainosho, Relayed anisotropy correlation NMR: determination of dihedral angles in solids, Chem. Phys. Lett. 256 (1996) 133–140.

[16] T. Fujiwara, T. Shimomura, H. Akutsu, Multidimensional solid-state nuclear magnetic resonance for correlating anisotropic interactions under magic-angle spinning conditions, J. Magn. Reson. 124 (1997) 147–153.

[17] M. Hong, J.D. Gross, R.G. Griffin, Site-resolved determination of peptide torsion angle ϕ from the relative orientation of backbone N–H and C–H bonds by solid-state NMR, J. Phys. Chem. B 101 (1997) 5869–5874.

[18] T. Fujiwara, T. Shimomura, Y. Ohigashi, H. Akutsu, Multidimensional solid-state nuclear magnetic resonance for determining the dihedral angle from the correlation of ^{13}C–^{1}H and ^{13}C–^{13}C dipolar interactions under magic-angle spinning conditions, J. Chem. Phys. 109 (1998) 2380–2393.

[19] X. Feng, P.J.E. Verdegem, M. Edén, D. Sandström, Y.K. Lee, P.H.M. Bovee-Geurts, W.J. de Grip, J. Lugtenburg, H.J.M. de Groot, M.H. Levitt, Determination of a molecular torsional angle in the metarhodopsin-I photointermediate of rhodopsin by double-quantum solid-state NMR, J. Biomol. NMR 16 (2000) 1–8.

[20] B. Reif, M. Hohwy, C.P. Jaroniec, C.M. Rienstra, R.G. Griffin, NH–NH vector correlation in peptides by solid-state NMR, J. Magn. Reson. 145 (2000) 132–141.

[21] K. Nomura, K. Takegoshi, T. Terao, K. Uchida, M. Kainosho, Three-dimensional structure determination of a uniformly labeled molecule by frequency-selective dipolar recouplingunder magic-angle spinning, J. Biomol. NMR 17 (2000) 111–123.

[22] R.G. Griffin, Dipolar recoupling in MAS spectra of biological solids, Nat. Struct. Biol. NMR Suppl. (1998) 508–512.

[23] M.H. Levitt, D.P. Raleigh, F. Creuzet, R.G. Griffin, Theory and simulations of homonuclear spin pair systems in rotating solids, J. Chem. Phys. 92 (1990) 6347–6364.

[24] T. Fujiwara, A. Ramamoorthy, K. Nagayama, K. Hioka, T. Fujito, Dipolar HOHAHA under MAS conditions for solid-state NMR, Chem. Phys. Lett. 212 (1993) 81–84.

[25] A.E. Bennett, C.M. Rienstra, J.M. Griffiths, W. Zhen, P.T. Lansbury Jr., R.G. Griffin, Homonuclear radio frequency-driven recoupling in rotating solids, J. Chem. Phys. 108 (1998) 9463–9479.

[26] T. Fujiwara, P. Khandelwal, H. Akutsu, Compound radio frequency-driven recoupling pulse sequence for efficient magneti-

zation transfer by homonuclear dipolar interaction under MAS conditions, J. Magn. Reson. 145 (2000) 73–83.
[27] G. Goobes, G.J. Boender, S. Vega, Spinning-frequency-dependent narrowband rf-driven dipolar recoupling, J. Magn. Reson. 146 (2000) 204–219.
[28] Y. Ishii, ^{13}C–^{13}C dipolar recoupling under very fast magic angle spinning in solid-state nuclear magnetic resonance: applications to distance measurements, spectral assignments, and high-throughput secondary-structure determination, J. Chem. Phys. 114 (2001) 8473–8483.
[29] N.C. Nielsen, H. Bildsøe, H.J. Jakobsen, M.H. Levitt, Double-quantum homonuclear rotary resonance: efficient dipolar recovery in magic-angle spinning nuclear magnetic resonance, J. Chem. Phys. 101 (1994) 1805–1812.
[30] Y.K. Lee, N.D. Kurur, M. Helmle, O.G. Johannessen, N.C. Nielsen, M.H. Levitt, Efficient dipolar recoupling in the NMR of rotating solids. A sevenfold symmetric radio-frequency pulse sequence, Chem. Phys. Lett. 242 (1995) 304–309.
[31] C.M. Rienstra, M.E. Hatcher, L.J. Mueller, B. Sun, S.W. Fesik, R.G. Griffin, Efficient multispin homonuclear double-quantum recoupling for magic-angle spinning NMR: ^{13}C–^{13}C correlation spectroscopy of U-^{13}C-erythromycin A, J. Am. Chem. Soc. 120 (1998) 10602–10612.
[32] M. Hohwy, H.J. Jakobsen, M. Edén, M.H. Levitt, N.C. Nielsen, Broadband dipolar recoupling in the nuclear magnetic resonance of rotating solids: a compensated C7 pulse sequence, J. Chem. Phys. 108 (1998) 2686–2694.
[33] M. Hohwy, C.M. Reinstra, C.P. Jaroniec, R.G. Griffin, Fivefold symmetric homonuclear dipolar recoupling in rotating solids: application to double quantum spectroscopy, J. Chem. Phys. 110 (1999) 7983–7991.
[34] M. Carravetta, M. Edén, X. Zhao, A. Brinkmann, M.H. Levitt, Symmetry principles for the design of radiofrequency pulse sequence in the nuclear magnetic resonance of rotating solids, Chem. Phys. Lett. 321 (2000) 205–215.
[35] A. Brinkmann, M. Edén, M.H. Levitt, Synchronous helical pulse sequences in magic-angle spinning nuclear magnetic resonance: double quantum recoupling of multiple-spin systems, J. Chem. Phys. 112 (2000) 8539–8554.
[36] I. Schnell, A. Watts, Towards selective recoupling and mutual decoupling of dipolar-coupled spin pairs in double-quantum magic-angle spinning NMR experiments on multiply labeled solid-state samples, Chem. Phys. Lett. 335 (2001) 111–122.
[37] R. Verel, M. Ernst, B.H. Meier, Adiabatic dipolar recoupling in solid-state NMR: the DREAM scheme, J. Magn. Reson. 150 (2001) 81–99.
[38] M. Edén, M.H. Levitt, Pulse sequence symmetries in the nuclear magnetic resonance of spinning solids: application to heteronuclear decoupling, J. Chem. Phys. 111 (1999) 1511–1519.
[39] A. Brinkmann, M.H. Levitt, Symmetry principles in the nuclear magnetic resonance of spinning solids: heteronuclear recoupling by generalized Hartmann–Hahn sequences, J. Chem. Phys. 115 (2001) 357–384.
[40] P.K. Madhu, X. Zhao, M.H. Levitt, High-resolution ^{1}H NMR in the solid state using symmetry-based pulse sequences, Chem. Phys. Lett. 346 (2001) 142–148.
[41] P.E. Kristiansen, D.J. Mitchell, J.N.S. Evans, Double-quantum dipolar recoupling at high magic-angle spinning rates, J. Magn. Reson. 157 (2002) 253–266.
[42] M. Baldus, A.T. Petkova, J. Herzfeld, R.G. Griffin, Cross polarization in the tilted frame: assignment and spectral simplification in heteronuclear spin systems, Mol. Phys. 95 (1998) 1197–1207.
[43] M. Hohwy, C.M. Rienstra, R.G. Griffin, Bandselective homonuclear dipolar recoupling in rotating solids, J. Chem. Phys. 117 (2002) 4973–4987.
[44] M. Mehring, Principles of High Resolution NMR in Solids, Springer, New York, 1983.
[45] C. Counsell, M.H. Levitt, R.R. Ernst, Analytical theory of composite pulses, J. Magn. Reson. 63 (1985) 133–141.
[46] M.H. Levitt, Composite pulses, Prog. Nucl. Magn. Reson. Spectrosc. 18 (1986) 61–122.
[47] T. Fujiwara, K. Nagayama, Efficiency of heteronuclear broadband decoupling and homonuclear *J* cross polarization analyzed on two time scales, J. Magn. Reson. 81 (1989) 245–254.
[48] A. Naito, S. Ganapathy, K. Akasaka, C.A. McDowell, Chemical shielding tensor and ^{13}C–^{14}N dipolar splitting in single crystals of L-alanine, J. Chem. Phys. 74 (1981) 3190–3197.
[49] M. Hong, Solid-state dipolar INADEQUATE NMR spectroscopy with a large double-quantum spectral width, J. Magn. Reson. 136 (1999) 86–91.
[50] A.S.D. Heindrichs, H. Geen, J.J. Titman, MAS double-quantum filtered dipolar shift correlation spectroscopy, J. Magn. Reson. 147 (2000) 68–77.
[51] G. Metz, X. Wu, S.O. Smith, Ramped-amplitude cross polarization in magic-angle-spinning NMR, J. Magn. Reson. A 110 (1994) 219–227.
[52] A.E. Bennett, C.M. Rienstra, M. Auger, K.V. Lakshmi, R.G. Griffin, Heteronuclear decoupling in rotating solids, J. Chem. Phys. 103 (1995) 6951–6958.
[53] L. Müller, R.R. Ernst, Coherence transfer in the rotating frame: application to heteronuclear cross-correlation spectroscopy, Mol. Phys. 38 (1979) 963–992.